How to cite: Angew. Chem. Int. Ed. 2024, e202318829
doi.org/10.1002/anie.202318829

Host-Guest Systems

Guest-Shuttling in a Nanosized Metallobox

Susana Ibáñez, Paula Salvà, Louise N. Dawe, and Eduardo Peris**

Abstract: An iridium-conjoined long and narrow metallorectangle was obtained by combining a quinoxalinophenanthrophenazine-connected Janus-di-imidazolylidene ligand and pyrazine. The size and shape of this assembly together with the fused polyaromatic nature of its panels provides it with properties that are uncommon for other metallosupramolecular assemblies. For example, this nanosized 'slit-like' metallobox is able show very large binding affinities with planar organic molecules in such a way, that the cavity is asymmetrically occupied by the guest molecule. This unsymmetrical conformation leads to the existence of a large amplitude motion of these guests, which slide between the two sides of the cavity of the host, thus constituting rare examples of molecular shuttles.

Introduction

During the last few years great effort has been devoted to the development of systems with the ability to work as molecular pumps and motors.[1] However, there is still a lack of studies regarding the quantitative information on the dynamics and mechanistic principles that control the motion within individual artificial molecular devices.[2] In order design supramolecular systems capable of performing specific movements, it is important to design artificial prototypes built with molecular components capable of moving in a controllable way, so that their study can provide a better understanding of the kinetic and thermodynamic constraints that determine their dynamic behavior.[1b] In this regard, during the last three decades, a great effort has been devoted to the design of molecular shuttles.[3] A molecular shuttle can be defined a prototypical artificial nanomachine that undergoes well-defined, large amplitude dynamics of one mechanically interlocked component with respect to the other.[4] This large amplitude translational motion was first described by Stoddart and co-workers in 1991.[5] The study of the dynamic behavior of molecular shuttles is extremely useful for the bottom-up molecular approach to molecular machines. So far, the field of molecular shuttles is largely dominated by rotaxane-like systems, so there is a need for developing other types of structures that may widen the scope of these prototypes and pave the way to more diverse machinery functions.

Poly-N-heterocyclic carbene ligands (NHCs) have recently appeared as very useful blocks for the construction of supramolecular organometallic complexes[6] and, in particular, those bridged by polycyclic aromatic hydrocarbons have shown interesting features regarding their host–guest chemistry properties.[7] During the last five years, we developed a large number of metallosquares[8] and metallorectangles[9] based on the use of a pyrene-bis-imidazolylidene ligand. The use of this Janus-di-NHC ligand,[10] allows a 'horizontal' metal-to-metal separation of 13 Å, so that the distance between the two cofacial parallel pyrene moieties can be modulated by using the appropriate pillars, or 'vertical' ligands (Scheme 1). The tetracationic metalloboxes **A**, **B** and **C** depicted in Scheme 1, can be regarded as the metallosupramolecular analogues of Stoddart's extended bipyridinium-based cationic cyclophanes,[11] which have shown strong donor-acceptor interactions forming host–guest complexes with various organic molecules when the size and electronic properties are adequately matched.

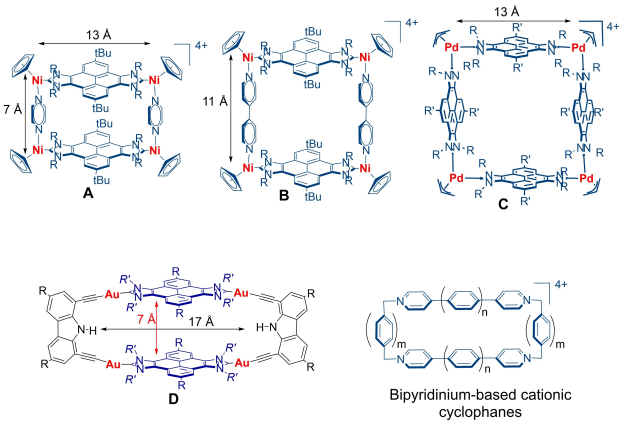

Scheme 1. Some selected organic and metallorganic box-like cyclophanes.

[*] Dr. S. Ibáñez, P. Salvà, Prof. E. Peris
Institute of Advanced Materials (INAM), Centro de Innovación en Química Avanzada (ORFEO-CINQA), Universitat Jaume I
Av. Vicente Sos Baynat s/n, Castellón, E-12006, Spain
E-mail: maella@uji.es
eperis@uji.es

Dr. L. N. Dawe
Department of Chemistry and Biochemistry, Wilfrid Laurier University, 75 University Avenue West, Waterloo, Ontario, N2 L 3 C5 Canada

The large library of existing Janus-di-NHC ligands in which the imidazolylidenes are connected by a variety of rigid polyaromatic linkers[10] constitutes a clear invitation for constructing a growing landscape of new metalloboxes with diverse architectures, so that the affinity profiles of these receptors can be tuned in a controllable manner by modifying the shape, size and electronic properties of the selected ligands. Built on these grounds, we herein describe the use of a nanosized Janus-di-NHC ligand with a quinoxalinophenanthrophenazine core,[12] for the construction of a two-nanometer long synthetic receptor. As will be described below, this long and narrow "slit-like" molecule displays two degenerate recognition sites, which can be used for the construction of an unusual type of molecular shuttle.

Results and Discussion

As it is depicted in Scheme 2, the reaction of quinoxalinophenanthrophenazine-bis-imidazolylidene di-iridium(I) complex **1**[12] with pyrazine, in the presence of two equivalents of $AgBF_4$ in CH_2Cl_2 leads to the air stable nanosized metallobox **2** in 66 % yield. Metallobox **2** was characterized by NMR, UV/Vis and fluorescence spectroscopy, and gave satisfactory elemental analysis. The Diffusion Ordered NMR spectrum (DOSY) of **2** shows that all proton resonances display the same diffusion coefficient in CD_2Cl_2 indicating that this species forms a single assembly (see Figure S32 in ESI). Unfortunately, the mass analysis of the complex via electrospray mass spectrometry (ESI-MS) allowed detection of only fragment ions generated from the thermal decomposition of the molecule, as a consequence of the relatively weak Ir(I)-N bonds.[13]

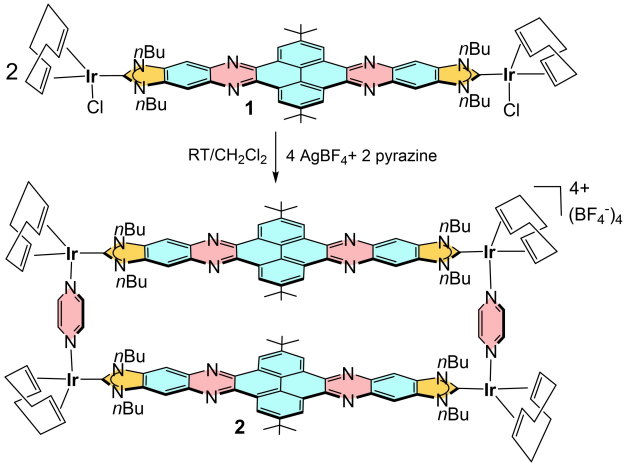

Scheme 2. Synthesis of metallobox **2**.

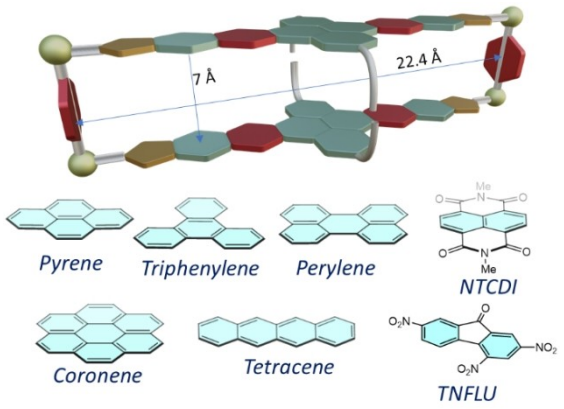

Scheme 3. Model of nanosized metallobox **2** and the different planar molecules used as guests in this study.

In order to test the host–guest chemistry properties of metallobox **2**, we performed a series of ^{1}H NMR titrations with a series of planar guests in CD_2Cl_2 (see Scheme 3). All the guests that we tested possess a planar structure, but also provide a wide scope in terms of shapes, composition and electronic nature. In general, the addition of solutions of the guests induced important perturbations in the ^{1}H NMR spectra. For all titrations, the addition of the guest induced the upfield shift of the two resonances due to the aromatic hydrogens of the horizontal polyaromatic panels, together with the downfield shift of the signal due to the protons of the pyrazine pillars. This observation confirms that the guests occupy the hollow gap of the metallobox, which is the only region where the chemical shift of the protons of the two linking ligands can be simultaneously perturbed. The titrations showed different kinetics depending on the nature of the guests used. For the case of the three smaller PAH guests (pyrene, triphenylene, tetracene and perylene), the titrations showed fast kinetics on the NMR timescale. On the contrary, the titrations performed with coronene, N,N′-dimethyl-naphthalenetetracarboxy-diimide (NTCDI) and 2,4,7-trinitro-9-fluorenone (TNFLU) showed slow kinetics on the NMR timescale, as two different species associated with the free host and the host:guest adducts were observed simultaneously upon addition of sub-stoichiometric amounts of guest to the CD_2Cl_2 solutions.

The ^{1}H NMR titrations allowed determination of the stoichiometry and the binding affinities for the formation of the host:guest adducts with pyrene, tryphenylene, perylene and tetracene, which are shown in Table 1. For the

Table 1: Association constants (M^{-1}) for the complexation of **2** with different organic and organometallic planar guests.

Entry	Guest	K_{11} (M^{-1})	K_{12} (M^{-1})	*NMR kinetics*
1	Pyrene[a]	385 ± 16	53 ± 3	Fast
2	Triphenylene[a]	1035 ± 85	155 ± 12	Fast
3	Tetracene[a]	3764 ± 243	—	Fast
4	Perylene[a]	5204 ± 278	—	Fast
5	Coronene[b]	176000 ± 6932	—	Slow
6	TNFLU[b]	199000 ± 5869	—	Slow
7	NTCDI[b]	306000 ± 8046	—	Slow

[a] K_{11} and K_{12} values calculated by global fitting analysis from ^{1}H NMR titrations, using a constant concentration of **2** (host) of 0,37 mM in CD_2Cl_2 at 298 K. [b] K_{11} values for coronene and NTCDI were calculated by UV/Vis titrations, using a constant concentration of **2** of 10^{-3} mM in CH_2Cl_2 at 298 K.

determination of the binding constants with coronene, NTCDI and TNFLU, we used UV/Vis titrations, since the slow kinetics and most of all, the large constants that could be inferred from the ^{1}H NMR titrations exceed the limits for being determined by NMR spectroscopic means.[14] For the encapsulation of the two smaller PAH guests (pyrene and triphenylene), we observed that the binding isotherms were best fitted to a 1:2 stoichiometric model, indicating that one molecule of **2** is capable of encapsulating two molecules of these smaller PAH guests. For these two guests the cooperative factor α (defined as $\alpha = 4\,K_{12}/K_{11}$) is less than 1, indicative of a negative cooperativity. This is most likely due to the steric congestion produced by the occupancy of two guest molecules in the cavity of **2**. For the rest of the guests (tetracene, perylene, coronene TNFLU and NTCDI), the binding isotherms were best fitted to a 1:1 stoichiometric model. The comparison of the binding constants allows to conclude that the binding affinities are in the order pyrene < triphenylene < tetracene < perylene < coronene < TNFLU < NTCDI. For the case of the planar PAHs, trend indicates that the affinities increase with the size and number of π-electrons of the guest,[9b,15] except for the case of tetracene, which shows a significantly larger binding constant than its isoelectronic molecule, triphenylene. This observation can be explained due to the accommodation of tetracene inside the cavity of **2**, in such a form that the longer axle of the guest would be aligned with the axle of the host, thus affording a more effective face-to-face overlap with the polyaromatic panels of the host than that shown by triphenylene. In the case of TNFLU and NTCDI, the large binding affinities are explained due to their electron-deficient nature (A), which makes the interaction with the pyrene containing panels of the host (D) form more stable stacks, as donor–acceptor–donor (D–A–D) interactions are known to be more favorable than donor–donor–donor (D–D–D) interactions.

The slow kinetics on the NMR timescale shown for the equilibria between **2** with coronene, NTCDI and TNFLU, together with the broad signals observed for the protons of the guest molecules, suggests that these three guests show a dynamic motion inside the cavity of the host. In order to shed some light into these dynamic processes, variable temperature ^{1}H NMR spectroscopic experiments were performed in CD_2Cl_2. As an illustrative example, Figure 1a shows the series of spectra obtained for the experiments performed with coronene@**2**. As can be observed in the series of spectra, at temperatures below 263 K the signals due to the protons of the benzene rings of the host (B, B′) start to split into two equal sets of signals that appear at 8.23 and 5.78 ppm. Similarly, the signals due to the protons of the pyrene panel of the host (C, C′), split into two set of signals (9.39 and 8.09 ppm) at temperatures below 253 K. Finally, the signals due to the protons of the pyrazine pillars (A, A′), split into two resonances (9.86 and 9.15 pm) at temperatures below 233 K. All these observations indicate the unsymmetrical nature of the frozen conformation of coronene@**2**, and suggest that the coronene guest is accommodated on one of the sides of the cavity of the host, closer to one of the pyrazine pillars, as illustrated in the schematic structure shown in Figure 1a. This asymmetric orientation of the guest inside the cavity of **2** is in full agreement with the X-ray diffraction molecular structure of complex coronene@**2**, as will be discussed below.

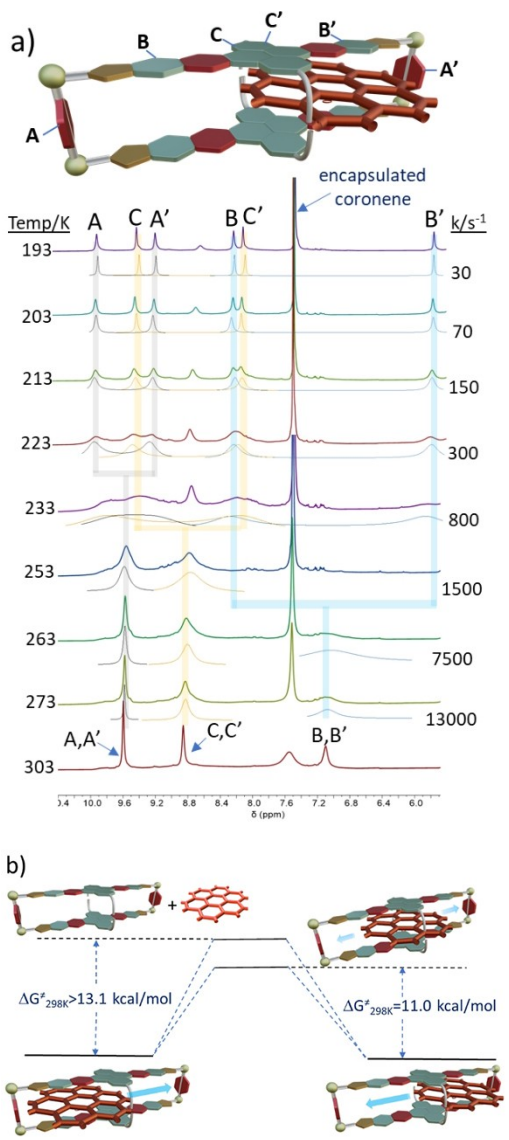

Figure 1. a) Study of the dynamic behaviour of coronene@**2** investigated by variable-temperature ^{1}H NMR spectroscopy. All spectra were recorded in CD_2Cl_2. The kinetic constants were determined using dynamic ^{1}H NMR line-shape simulations. The simulated spectra are shown below the experimental ones. b) Schematic kinetic profiles for the intramolecular dynamic exchange observed for coronene@**2**, considering the two possible mechanisms: guest shuttling (intramolecular) and guest release-uptake (intermolecular).

The orientation of the guest on one of the sides of the cavity indicates that there are two possible degenerate conformations, as the molecule of coronene can occupy either side of the cavity of the host. ^{1}H NMR line-shape simulations of the spectra shown in Figure 1a allowed us to estimate the rate constants at different temperatures. An Eyring plot was used to estimate the $\Delta H^{\neq}$ and $\Delta S^{\neq}$ values, which were 7.7 ± 0.3 kcal/mol and -11 ± 0.3 cal/molK, re-

spectively (see Figure S30 in ESI), so that the activation Gibbs energy for the sliding of the coronene guest along the cavity is determined to be $\Delta G^{\neq}_{298K} = 11.0$ kcal/mol. It is important to mention that the activation Gibbs energy determined for this mechanism is significantly lower than that shown by the exchange of the free/encapsulated guest, which as mentioned above shows slow kinetics on the NMR timescale. The $\Delta\nu$ separation between the resonances due to free and encapsulated coronene is $\Delta\nu = 700$ Hz, so the Gibbs energy at the coalescence temperature is 13.1 kcal/mol. Given that 298K lies below the coalescence temperature for this exchange (the coalescence temperature could not be reached below the limit temperature established by the boiling point of CD_2Cl_2), we can establish that the activation barrier for guest exchange at 298K is >13.1 kcal mol. This means that the movement of the guest from one side of the cavity to the other must be intramolecular, as a consequence of the sliding of the guest from one side to the other. The energy profiles for the intramolecular (guest shuttling) and intermolecular (reversible guest release) mechanisms are schematically depicted in Figure 1b. For this sliding mechanism, the enthalpy cost to form the transition state may arise from the conformational distortion of the host when the guest passes through the middle part of the metallorectangle, as the two pyrene panels of the host need to separate to facilitate the sliding of the planar guest in order to avoid the steric clash of the guest with the *tert*-butyl groups at the pyrene panels. Thus, these *tert*-butyl groups play the role of steric "speed bumps" that limit the rate of the transitions between the two degenerate recognition sites. Very likely the absence of these bulky groups would accelerate the exchange. In addition, the loss of the C-H···π interaction between the guest and the pyrazine rings (as reflected by the X-ray molecular structure of the complex, which is described below), should also contribute to this positive activation enthalpy. The negative entropy indicates that the transition state is more solvated that the ground state.

For the case of NTCDI@**2**, a VT ^{1}H NMR study was also performed (see Figures S32 and S33 in ESI), which lead to similar conclusions. The experiment suggests that, as happened with the coronene guest, the molecule of NTCDI is accommodated on one of the sides of the cavity, thus rendering two degenerate conformations that show a dynamic exchange. The trapped NTCDI molecule shuttles between the two sides of the metallobox. The kinetic data obtained from the analysis of the variable temperature ^{1}H NMR experiments were $\Delta H^{\neq} = 8.1 \pm 0.1$ kcal/mol and $\Delta S^{\neq} = -5.2 \pm 0.6$ cal/molK (see Figure S33 in ESI for details). As will be discussed later, the accommodation of the guest on one of the sides of the cavity in NTCDI@**2** is also confirmed by the X-ray diffraction solid-state structure.

Single crystals of coronene@**2**, NTCDI@**2** and TNFLU@**2** suitable for X-ray diffraction studies were obtained by slow diffusion of hexane into a concentrated solution of the complex in chloroform (Figure 2).[16] The molecular structure of coronene@**2** (Figure 2a) consists of a tetra-iridium rectangle with two cofacial quinoxalinophenanthrophenazine-bis-imidazolylidene ligands and two pyrazine ligands that constitute the long and short sides of the rectangle, respectively. One molecule of coronene is trapped inside the cavity of the metallorectangle and located on one of its sides, close to one of the pyrazine pillars, and one of the hydrogen atoms of the coronene guest forms CH···π interactions with the pyrazine pillar, as shown by the distance of 2.74 Å between this hydrogen atom and the centroid of the pyrazine ring. The asymmetric disposition of the molecule of coronene is in full agreement with the variable temperature ^{1}H NMR experiments, as it justifies the splitting of the signals due to the protons of the quinoxalinophenanthrophenazine core of the host molecule for the 'frozen' structure of the complex. The centroid of the coronene molecule is aligned with the two centroids of the two cofacial pyrazine rings of the quinoxalinophenanthrophenazine core. The separation between the iridium atoms connected by the bis-NHC ligand measures 22.6 Å, while

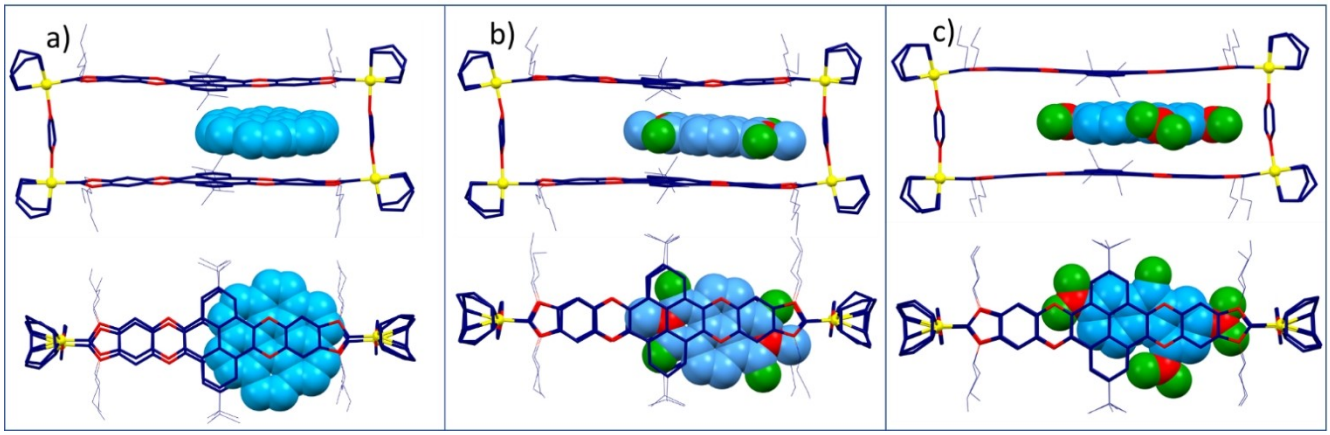

Figure 2. Two perspectives of the molecular structure of coronene@**2** (a), NTCDI@**2** (b) and TNFLU@**2** (c), obtained from single-crystal X-ray diffraction studies. Hydrogen atoms are omitted from the Figure for clarity. Counter anions (BF_4^-) and solvent molecules ($CHCl_3$) were excluded from the model using a solvent mask. Carbon atoms are shown in blue, nitrogen atoms in red, oxygen atoms in green and iridium atoms in yellow. For clarity, only one disordered orientation of the NTCDI and TNFLU guests in NTCDI@**2** and TNFLU@**2** are displayed.

the distance between the two pyrazine connected iridium centers is 6.9 Å. The distance between the two centroids of the parallel pyrazine bridging ligands is of 22.3 Å. The 'height' (distance between the two cofacial long polyaromatic ligands) of the host is quite homogeneous all along the length of the quinoxalinophenanthrophenazine-bis-imidazolylidene ligand, as reflected by the distances between the centroids of the benzene-pyrazine rings close to the coronene, the pyrene moieties, and the benzene-pyrazine rings on the empty side of the host, which are 6.98, 6.83 and 7.16 Å, respectively. This negligible deviation from the ideal distance of 7 Å for the 'vertical' size of molecule along its longer horizontal axle is an indication of the excellent size match between the host and the coronene guest. This also helps to explain the very large binding affinity between these two molecules, as trapping the molecule of coronene seems to not have any energy cost due to conformational distortions of the host molecule. The molecular structure of NTCDI@**2** (Figure 2b) shows that one molecule of NTCDI is trapped inside the cavity of the metallorectangle and has adopted two superimposed (same plane) slipped geometries, with equal (half) occupancies, both located close to a single pyrazine pillar. For simplicity, only one of NTCDI molecules is shown in Figure 2b. Again, the asymmetric disposition of the molecule of NTCDI agrees with the variable temperature ^{1}H NMR experiments. The observed separation between the iridium atoms connected by the bis-NHC ligand is 22.6 Å, while the distance between the two pyrazine connected iridium centers is 6.9 Å. The 'height' of the host is on average 6.97 Å. The NTCDI plane-centroid to quinoxalinophenanthrophenazine core plane distances were 3.467(6) and 3.472(5) Å ('top' and 'bottom' contacts) with twist/fold angles between each plane of less than 5°. The molecular structure of TNFLU@**2** (Figure 2c) shows that one molecule of TNFLU is trapped inside the cavity of the metallorectangle and has adopted two superimposed (same plane) slipped geometries, with equal (0.25) occupancies. Both orientations are further superimposed on an inversion center, yielding four orientations of TNFLU per metallorectangle. The distance between the iridium atoms connected by the bis-NHC ligand is 22.6 Å, while the distance between the two pyrazine connected iridium centers is 6.9 Å. The 'height' of the host is on average 6.95 Å. The TNFLU plane-centroid to quinoxalinophenanthrophenazine core plane distances were 3.4096(15) and 3.4271(16) Å ('top' and 'bottom' contacts) with twist/fold angles between each plane of less than 9°.

Conclusion

In summary, we described a nanosized metallorectangle that behaves as a very versatile receptor capable of binding planar electron-rich polycyclic aromatic hydrocarbons and electron-deficient guests such as NTCDI and TNFLU. The fact that this molecule can be obtained in high yield from a relatively simple synthetic procedure constitutes an advantage compared to the preparation of other symmetry-related organic-based cationic cyclophanes. The long and shallow shape of the cavity of this molecular rectangle (22.6×7 Å^2), together with the fused polyaromatic nature of its panels provides it with interesting properties that are uncommon for other types of metallosupramolecular assemblies. For example, we showed that **2** is able to form ternary complexes by encapsulating two small PAH guests, such as pyrene and triphenylene. More interesting is the fact that planar molecules such as coronene, NTCDI and TNFLU form kinetically stable complexes, so this type of receptor also invites to explore potential applications related to thermodynamic versus kinetic complexation. In fact, coronene@**2**, NTCDI@**2** and TNFLU@**2** show dynamic behaviors, in which the guest molecule shows a wide amplitude translational motion from one side of the cavity to the other, thus displaying the type of dynamic behavior which is typically ascribed to molecular shuttles. Our new metallobox is complex enough for accomplishing a challenging function, but also simple enough to allow a thorough analysis using standard kinetic and thermodynamic models of chemistry. The fact that the nature of the guest determines the dynamic behavior of the resulting host:guest complex invites for further investigations which may be useful for fine-tuning the motions of guests inside their hosts and for paving the way for developing organometallic-based molecular machines.

Supporting Information

The Supporting Information file contains all the experimental details dealing with the characterization, calculation of binding affinities and X-ray diffraction details. This includes all NMR spectra, and description of methods for determining the association constants, observed kinetic constants and thermodynamic parameters.

The authors have cited additional references within the Supporting Information.[17]

Acknowledgements

We gratefully acknowledge financial support from the Ministerio de Ciencia y Universidades (PID2021-127862NB-I00), Generalitat Valenciana (CIPROM/2021/079) and the Universitat Jaume I (UJI-B2020-01). We are grateful to the Serveis Centrals d'Instrumentació Científica (SCIC-UJI) for providing with spectroscopic facilities. We are very thankful to Dr. Macarena Poyatos for her valuable contribution to the study.

Conflict of Interest

The authors declare no conflict of interest.

Data Availability Statement

The data that support the findings of this study are available in the supplementary material of this article.

Keywords: Host-Guest Chemistry · Molecular Shuttles · N-Heterocyclic Carbenes · Polycyclic Aromatic Hydrocarbons · Supramolecular Organometallic Complexes

[1] a) S. Erbas-Cakmak, D. A. Leigh, C. T. McTernan, A. L. Nussbaumer, *Chem. Rev.* **2015**, *115*, 10081–10206; b) S. Silvi, M. Venturi, A. Credi, *J. Mater. Chem.* **2009**, *19*, 2279–2294; c) S. Kassem, T. van Leeuwen, A. S. Lubbe, M. R. Wilson, B. L. Feringa, D. A. Leigh, *Chem. Soc. Rev.* **2017**, *46*, 2592–2621.

[2] C. Pezzato, C. Cheng, J. F. Stoddart, R. D. Astumian, *Chem. Soc. Rev.* **2017**, *46*, 5491–5507.

[3] a) S. Saha, A. H. Flood, J. F. Stoddart, S. Impellizzeri, S. Silvi, M. Venturi, A. Credi, *J. Am. Chem. Soc.* **2007**, *129*, 12159–12171; b) J. D. Crowley, S. M. Goldup, A. L. Lee, D. A. Leigh, R. T. McBurney, *Chem. Soc. Rev.* **2009**, *38*, 1530–1541; c) K. L. Zhu, C. A. O'Keefe, V. N. Vukotic, R. W. Schurko, S. J. Loeb, *Nat. Chem.* **2015**, *7*, 514–519; d) T. A. Barendt, A. Docker, I. Marques, V. Félix, P. D. Beer, *Angew. Chem. Int. Ed.* **2016**, *55*, 11069–11076; e) J. F. Stoddart, *Angew. Chem. Int. Ed.* **2017**, *56*, 11094–11125; f) V. N. Vukotic, K. L. Zhu, G. Baggi, S. J. Loeb, *Angew. Chem. Int. Ed.* **2017**, *56*, 6136–6141; g) B. H. Wilson, L. M. Abdulla, R. W. Schurko, S. J. Loeb, *Chem. Sci.* **2021**, *12*, 3944–3951; h) Y.-P. Tang, Y.-E. Luo, J.-F. Xiang, Y.-M. He, Q.-H. Fan, *Angew. Chem. Int. Ed.* **2022**, *61*, e202200638; i) A. Dhara, A. Dmitrienko, R. N. N. Hussein, A. Sotomayor, B. H. H. Wilson, S. J. J. Loeb, *Chem. Sci.* **2023**, *14*, 7215–7220; j) M. Gauthier, K. Fournel-Marotte, C. Clavel, P. Waeles, P. Laurent, F. Coutrot, *Angew. Chem. Int. Ed.* **2023**, *62*, e202310643–e202310643; k) J. D. Crowley, D. A. Leigh, P. J. Lusby, R. T. McBurney, L.-E. Perret-Aebi, C. Petzold, A. M. Z. Slawin, M. D. Symes, *J. Am. Chem. Soc.* **2007**, *129*, 15085–15090.

[4] S. Chen, D. Su, C. Jia, Y. Li, X. Li, X. Guo, D. A. Leigh, L. Zhang, *Chem* **2022**, *8*, 243–252.

[5] P. L. Anelli, N. Spencer, J. F. Stoddart, *J. Am. Chem. Soc.* **1991**, *113*, 5131–5133.

[6] a) M. M. Gan, J. Q. Liu, L. Zhan, Y. Y. Wang, F. E. Hahn, Y. F. Han, *Chem. Rev.* **2018**, *118*, 9587–9641; b) N. Sinha, F. E. Hahn, *Acc. Chem. Res.* **2017**, *50*, 2167–2184; c) S. Bai, Y. F. Han, *Acc. Chem. Res.* **2023**, *56*, 1213-1227; d) A. Pöthig, A. Casini, *Theranostics* **2019**, *9*, 3150–3169; e) Y. Lu, P. D. Dutschke, J. Kinas, A. Hepp, G.-X. Jin, F. E. Hahn, *Angew. Chem. Int. Ed.* **2023**, *62*, e202217681.

[7] S. Ibáñez, M. Poyatos, E. Peris, *Acc. Chem. Res.* **2020**, *53*, 1401–1413.

[8] V. Martinez-Agramunt, T. Eder, H. Darmandeh, G. Guisado-Barrios, E. Peris, *Angew. Chem. Int. Ed.* **2019**, *58*, 5682–5686.

[9] a) S. Ibáñez, E. Peris, *Angew. Chem. Int. Ed.* **2020**, *59*, 6860–6865; b) V. Martinez-Agramunt, S. Ruiz-Botella, E. Peris, *Chem. Eur. J.* **2017**, *23*, 6675–6681; c) S. Ibáñez, K. Swiderek, E. Peris, *Angew. Chem. Int. Ed.* **2023**, *62*, e202301914.

[10] M. Poyatos, E. Peris, *Dalton Trans.* **2021**, *50*, 12748–12763.

[11] E. J. Dale, N. A. Vermeulen, M. Juricek, J. C. Barnes, R. M. Young, M. R. Wasielewski, J. F. Stoddart, *Acc. Chem. Res.* **2016**, *49*, 262–273.

[12] H. Valdés, M. Poyatos, E. Peris, *Organometallics* **2015**, *34*, 1725–1729.

[13] a) K. Yamaguchi, *Mass Spectrom (Tokyo)* **2013**, *2*, S0012; b) K. Yamaguchi, *J. Mass Spectrom.* **2003**, *38*, 473–490.

[14] a) A. J. Lowe, F. M. Pfeffer, P. Thordarson, *Supramol. Chem.* **2012**, *24*, 585–594; b) P. Thordarson, *Chem. Soc. Rev.* **2011**, *40*, 1305–1323.

[15] a) E. J. Dale, N. A. Vermeulen, A. A. Thomas, J. C. Barnes, M. Juricek, A. K. Blackburn, N. L. Strutt, A. A. Sarjeant, C. L. Stern, S. E. Denmark, J. F. Stoddart, *J. Am. Chem. Soc.* **2014**, *136*, 10669–10682; b) J. C. Barnes, M. Juricek, N. L. Strutt, M. Frasconi, S. Sampath, M. A. Giesener, P. L. McGrier, C. J. Bruns, C. L. Stern, A. A. Sarjeant, J. F. Stoddart, *J. Am. Chem. Soc.* **2013**, *135*, 183–192.

[16] Deposition numbers 2293189 (for coronene@**2**), 2293188 (for NTCDI@**2**) and 2312684 (for TNFLU@**2**) contain the supplementary crystallographic data for this paper. These data are provided free of charge by the joint Cambridge Crystallographic Data Centre and Fachinformationszentrum Karlsruhe Access Structures service.

[17] a) K. M. C. Wong, L. L. Hung, W. H. Lam, N. Y. Zhu, V. W. W. Yam, *J. Am. Chem. Soc.* **2007**, *129*, 4350–4365; b) O. V. Dolomanov, L. J. Bourhis, R. J. Gildea, J. A. K. Howard, H. Puschmann, *J. Appl. Crystallogr.* **2009**, *42*, 339–341; c) G. M. Sheldrick, *Acta Crystallogr. Sect. A* **2008**, *64*, 112–122; d) G. M. Sheldrick, *Acta Crystallogr. Sect. A* **2015**, *71*, 3–8; e) P. van der Sluis, A. L. Spek, *Acta Crystallogr. Sect. A* **1990**, *46*, 194–201; f) A. L. Spek, *J. Appl. Crystallogr.* **2003**, *36*, 7–13.

Manuscript received: December 7, 2023
Accepted manuscript online: January 5, 2024
Version of record online: ■■, ■■

Research Articles

Host-Guest Systems

S. Ibáñez,* P. Salvà, L. N. Dawe, E. Peris* ——— e202318829

Guest-Shuttling in a Nanosized Metallobox

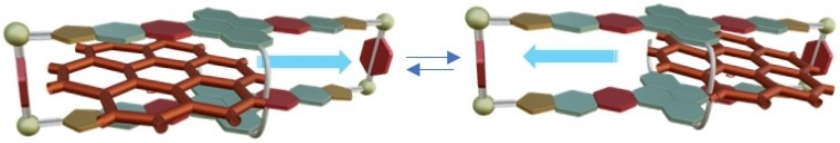

A two-nanometer long iridium-cornered metallorectangle was obtained and used for the encapsulation of a wide variety of planar guests. This slit-shaped metallobox is able to form host–guest complexes with a variety of planar molecules, which slide from one side of the cavity to the other, with a large amplitude motion that was experimentally quantified.